




## Abnormal phonon angular momentum due to off-diagonal elements in the density matrix induced by a temperature gradient

Jinxin Zhong,<sup>1,\*</sup> Hong Sun,<sup>2,\*</sup> Yang Pan,<sup>2</sup> Zhiguo Wang<sup>1</sup> ,<sup>1</sup> Xiangfan Xu,<sup>1</sup> Lifa Zhang,<sup>2,†</sup> and Jun Zhou<sup>1,2,‡</sup> 

<sup>1</sup>*School of Physics Science and Engineering, Tongji University, Shanghai 200092, China*

<sup>2</sup>*Phonon Engineering Research Center of Jiangsu Province, Center for Quantum Transport and Thermal Energy Science, Institute of Physics and Interdisciplinary Science, School of Physics and Technology, Nanjing Normal University, Nanjing 210023, China*

 (Received 31 July 2022; revised 28 December 2022; accepted 15 March 2023; published 24 March 2023)

A temperature gradient in chiral materials can generate a nonzero mean value of phonon angular momentum (PAM). We used the Kubo formula to investigate the contribution of both intraband and interband terms of PAM to the mean PAM. Interestingly, the interband term was found to be as important as the intraband term, indicating that the quantum transition between different phonon branches induced by a temperature gradient strongly affects locally atomic rotation. This discovery opens up an alternative mechanism for generating PAM and phonon magnetic moments.

DOI: [10.1103/PhysRevB.107.125147](https://doi.org/10.1103/PhysRevB.107.125147)

### I. INTRODUCTION

Phonons are the quanta of atomic displacement fields in solids [1]. For a lattice with a given structure and force constants, one can write the dynamical matrix  $\mathbf{D}(\mathbf{k})$ , where  $\mathbf{k}$  is the phonon wave vector. According to the lattice dynamics [2,3], the displacement of each atom can be obtained through solving the equations of motion which contain  $\mathbf{D}(\mathbf{k})$ . When the lattice has inversion symmetry,  $\mathbf{D}(\mathbf{k})$  is a real matrix and  $\mathbf{D}(\mathbf{k}) = \mathbf{D}(-\mathbf{k})$ . Consequently, the polarization vectors  $\epsilon_{\mathbf{k}\sigma}$  must be real, where  $\sigma$  is the branch index, and the system contains only linear polarization. In contrast, when the inversion symmetry is broken,  $\mathbf{D}(\mathbf{k})$  is a complex matrix and  $\epsilon_{\mathbf{k}\sigma}$  could be complex. Then the system contains not only vibration but also rotation [4,5].

Classically, the displacement of an atom in the unit cell  $l$  at  $\mathbf{R}_l$  is  $\mathbf{u}_l \sim \text{Re}[\epsilon_{\mathbf{k}\sigma} e^{i(\mathbf{k}\cdot\mathbf{R}_l - \omega_{\mathbf{k}\sigma}t)}]$  for a given state  $(\sigma, \mathbf{k})$  [1], where  $\omega_{\mathbf{k}\sigma}$  is the phonon frequency. For the real polarization vector,  $\mathbf{u}_l \sim \epsilon_{\mathbf{k}\sigma} \cos(\mathbf{k}\cdot\mathbf{R}_l - \omega_{\mathbf{k}\sigma}t)$ . The motion of the atom can be regarded as three “*in-phase*” harmonic oscillators which give rise to zero angular momentum because  $\mathbf{u}_l$  is always parallel to  $\dot{\mathbf{u}}_l$ . The case is different for complex polarization vectors, the displacement along the  $\mu$  direction ( $\mu, \nu, \alpha, \gamma = x, y, z$ ) is

$$u_l^\mu \sim \text{Re}(\epsilon_{\mathbf{k}\sigma}^\mu) \cos(\mathbf{k}\cdot\mathbf{R}_l - \omega_{\mathbf{k}\sigma}t) - \text{Im}(\epsilon_{\mathbf{k}\sigma}^\mu) \times \sin(\mathbf{k}\cdot\mathbf{R}_l - \omega_{\mathbf{k}\sigma}t) = \cos(\mathbf{k}\cdot\mathbf{R}_l - \omega_{\mathbf{k}\sigma}t + \phi_{\mathbf{k}\sigma}^\mu), \quad (1)$$

where the phase shift is determined by  $\tan(\phi_{\mathbf{k}\sigma}^\mu) = \text{Im}(\epsilon_{\mathbf{k}\sigma}^\mu)/\text{Re}(\epsilon_{\mathbf{k}\sigma}^\mu)$ . Equation (1) shows that the motion of the atom can be regarded as three harmonic oscillators with the

phase difference  $\phi_{\mathbf{k}\sigma}^\mu - \phi_{\mathbf{k}\sigma}^\nu$ , where  $\mu \neq \nu$ . In other words, atoms rotate around their equilibrium positions circularly or elliptically. The microscopic local rotation gives rise to nonzero angular momentum, which has been experimentally observed in WSe<sub>2</sub> [6]. Such angular momentum is called the phonon angular momentum (PAM) [7,8].

A quantum mechanical theory of PAM was first given by McLellan [9]. The overall PAM of a lattice with  $n_a$  atoms in each unit cell can be written as [9]

$$\mathbf{L} = \sum_{l\kappa} \mathbf{u}_{l\kappa} \times (m_\kappa \dot{\mathbf{u}}_{l\kappa}), \quad (2)$$

where  $m_\kappa$  is the mass of the  $\kappa$ th atom with  $\kappa = 1, 2, \dots, n_a$ . In 2014, Zhang and Niu [7] presented a comprehensive second quantization form of PAM when the inversion symmetry is absent. They found that, when the system is in equilibrium and has time-reversal symmetry, the mean PAM vanishes. A nonzero mean PAM can be obtained by two possible ways: (i) breaking the time-reversal symmetry [7,10–13] and (ii) driving the system into nonequilibrium [14–16]. Later on, Hamada *et al.* [14] found a nonzero PAM by using the Boltzmann transport equation under the relaxation time approximation when a temperature gradient was applied. The  $\mu$  component of the mean PAM is calculated as  $\langle L_\mu \rangle = \Lambda_{\mu\nu} (\nabla T)_\nu$ , where  $\Lambda_{\mu\nu}$  is a response tensor. As a result, a nonzero phonon magnetic moment due to PAM can be calculated accordingly [14,15,17].

According to Hamada *et al.*'s calculation [14], the phonon magnetic moment was expected to be much smaller than the Bohr magneton. However, experiments have shown that certain materials, such as the Dirac semimetal Cd<sub>3</sub>As<sub>2</sub> [18] and ErFeO<sub>3</sub> [19], exhibit a much larger phonon magnetic moment [20,21]. In particular, Cd<sub>3</sub>As<sub>2</sub>'s phonon magnetic moment was found to be 2.7 times greater than the Bohr magneton [18]. This result may be due to contributions from the phonon-modified electronic energy together with the momentum-space Berry curvature [17]. Recently, ultrafast

\*These authors contributed equally to this work.

†phyzlf@njnu.edu.cn

‡zhoujunzhou@njnu.edu.cn

demagnetization experiments have shown that crystals can rapidly lose electron spin angular momentum to phonons [22]. This suggests that phonons can produce magnetic moments comparable to those of electrons through circular polarization. Moreover, Kim *et al.* [23] observed a chiral-phonon-activated spin Seebeck effect in a chiral organic-inorganic hybrid perovskite through an ultrafast pump-probe experiment. It possibly provides evidence that PAM can activate a strong magnetic moment. Therefore, there may be other mechanisms beyond Hamada *et al.*'s calculation [14] that could contribute to an additional mean PAM and phonon magnetic moment. For example, Xiong *et al.* [24] recently used the Biot Savart law to find that the effective magnetic fields induced by chiral phonons in the point-charge model could reach 0.01 T at room temperature. In addition, we note that none of the previous studies have considered the effect of interband phonon transitions.

In this work, we revisit the derivation from Eq. (2) and propose an alternative mechanism to generate a nonzero mean PAM by keeping both diagonal terms (which describe intraband phonon transition) and off-diagonal terms (which describe interband phonon transition) of the density matrix in the Kubo formula. We find that the interband terms of PAM result in a notable mean PAM.

## II. PHONON ANGULAR MOMENTUM OPERATOR

We start our study from the  $\mu$  component of Eq. (2), which can be written as [25]

$$L_\mu \approx \frac{\hbar}{2N} \sum_l \sum_{\mathbf{k}, \mathbf{k}'} \sum_{\sigma, \sigma'} \left( \epsilon_{\mathbf{k}\sigma}^\dagger M_\mu \epsilon_{\mathbf{k}'\sigma'} \sqrt{\frac{\omega_{\mathbf{k}'\sigma'}}{\omega_{\mathbf{k}\sigma}}} a_{\mathbf{k}\sigma}^\dagger a_{\mathbf{k}'\sigma'} - \epsilon_{\mathbf{k}'\sigma'}^T M_\mu \epsilon_{\mathbf{k}\sigma}^* \sqrt{\frac{\omega_{\mathbf{k}\sigma}}{\omega_{\mathbf{k}'\sigma'}}} a_{\mathbf{k}'\sigma'}^\dagger a_{\mathbf{k}\sigma} \right) e^{i\mathbf{R}_l \cdot (\mathbf{k}' - \mathbf{k})}. \quad (3)$$

Here  $M_\mu = I_{n_a \times n_a} \otimes (-i)\epsilon_{\mu\nu\gamma}$  ( $\epsilon$  is Levi-Civita tensor),  $\hbar$  is the Planck constant,  $N$  is the number of unit cells, and  $a_{\mathbf{k}\sigma}^\dagger$  and  $a_{\mathbf{k}\sigma}$  are the creation and annihilation operators of phonons, respectively. Both  $aa$  and  $a^\dagger a^\dagger$  terms are neglected since they vary rapidly with time and have marginal contribution. When the system is a crystal, Eq. (3) can be further simplified by  $\frac{1}{N} \sum_l e^{i\mathbf{R}_l \cdot (\mathbf{k}' - \mathbf{k})} = \delta_{\mathbf{k}, \mathbf{k}'}$  and  $-\epsilon_{\mathbf{k}'\sigma'}^T M_\mu \epsilon_{\mathbf{k}\sigma}^* = \epsilon_{\mathbf{k}\sigma}^\dagger M_\mu \epsilon_{\mathbf{k}'\sigma'}$ . Using the commutation relation  $[a_{\mathbf{k}\sigma'}, a_{\mathbf{k}\sigma}^\dagger] = \delta_{\sigma\sigma'}$ ,  $L_\mu$  can be divided into two parts, the diagonal term ( $L_\mu^D$ ) and the off-diagonal term ( $L_\mu^{\text{OD}}$ ), as follows:

$$L_\mu^D = \sum_{\mathbf{k}\sigma} l_{\mathbf{k}\sigma}^\mu \left[ a_{\mathbf{k}\sigma}^\dagger a_{\mathbf{k}\sigma} + \frac{1}{2} \right], \quad (4a)$$

$$L_\mu^{\text{OD}} = \sum_{\mathbf{k}} \sum_{\substack{\sigma \neq \sigma' \\ \sigma \sigma'}} l_{\mathbf{k}\sigma\sigma'}^\mu a_{\mathbf{k}\sigma}^\dagger a_{\mathbf{k}\sigma'}. \quad (4b)$$

We note the matrix elements in Eqs. (4a) and (4b) as

$$l_{\mathbf{k}\sigma}^\mu = \hbar(\epsilon_{\mathbf{k}\sigma}^\dagger M_\mu \epsilon_{\mathbf{k}\sigma}), \quad (5a)$$

$$l_{\mathbf{k}\sigma\sigma'}^\mu = \frac{\hbar}{2} \epsilon_{\mathbf{k}\sigma}^\dagger M_\mu \epsilon_{\mathbf{k}\sigma'} \left( \sqrt{\frac{\omega_{\mathbf{k}\sigma'}}{\omega_{\mathbf{k}\sigma}}} + \sqrt{\frac{\omega_{\mathbf{k}\sigma}}{\omega_{\mathbf{k}\sigma'}}} \right), \quad \sigma \neq \sigma'. \quad (5b)$$

The diagonal term in Eq. (4a) and its matrix elements in Eq. (5a) have been studied in our previous work [7]. The off-

diagonal term in Eq. (4b) and its matrix elements in Eq. (5b) show that the interband terms of PAM describe the quantum transition between state  $(\sigma, \mathbf{k})$  and state  $(\sigma', \mathbf{k})$ .

## III. KUBO FORMULA AND HEAT CURRENT OPERATOR

We modify the Kubo formula of thermal conductivity [26–28], which is similar to the electrical Kubo formula [29], to calculate a frequency-dependent mean PAM. The thermal Kubo formula [26] is different from the electrical Kubo formula [29]. The reason is that there is a well-defined external force which drives the electrical current. In contrast, there is no similar term involving the temperature gradient in the Hamiltonian to drive a heat current. Thus the thermal Kubo formula requires an additional statistical hypothesis [27,28], which assumes a local space-dependent temperature  $T(x) = [k_B \beta(x)]^{-1}$ . Then the local density matrix is

$$\rho = \frac{e^{-\int d^3x \beta(x) h(x)}}{Z}, \quad (6)$$

where  $h(x)$  is the Hamiltonian density operator,  $Z$  is the partition function, and the Hamiltonian  $H = \int d^3x h(x)$ . A heat current density operator  $\mathbf{S}(x)$  is now defined by the condition of local energy conservation:

$$\frac{\partial h(x)}{\partial t} + \nabla \cdot \mathbf{S}(x) = 0. \quad (7)$$

The total heat current operator is  $\mathbf{S} = \frac{1}{V} \int d^3x \mathbf{S}(x)$ , where  $V$  is the volume. Hardy [30] has shown that the quadratic terms of the heat current operator are

$$\mathbf{S} = \frac{1}{2V} \sum_{l'l'} \sum_{\kappa\kappa'} (\mathbf{R}_{l\kappa} - \mathbf{R}_{l'\kappa'}) \sum_{\alpha} \left\{ \frac{p_{l\kappa\alpha}}{m_\kappa} \frac{1}{i\hbar} [p_{l\kappa\alpha}, V(\mathbf{R}_{l'\kappa'})] + \frac{1}{i\hbar} [p_{l\kappa\alpha}, V(\mathbf{R}_{l'\kappa'})] \frac{p_{l\kappa\alpha}}{m_\kappa} \right\}, \quad (8)$$

where  $V(\mathbf{R}_{l'\kappa'})$  is the harmonic potential energy

$$V(\mathbf{R}_{l'\kappa'}) = \frac{1}{2} \sum_l \sum_{\kappa} \sum_{\alpha\gamma} \Phi_{\alpha\gamma}(l\kappa, l'\kappa') u_{l\kappa\alpha} u_{l'\kappa'\gamma}. \quad (9)$$

$\Phi$  is the force constant matrix. It is easy to verify that  $\frac{1}{i\hbar} [p_{l\kappa\alpha}, V(\mathbf{R}_{l'\kappa'})] = -\frac{1}{2} \sum_{\beta} \Phi_{\alpha\gamma}(l\kappa, l'\kappa') u_{l'\kappa'\gamma}$ , and then

$$\mathbf{S} = \frac{1}{2V} \sum_{l'l'} \sum_{\kappa\kappa'} \sum_{\alpha\gamma} (\mathbf{R}_{l'\kappa'} - \mathbf{R}_{l\kappa}) \Phi_{\alpha\gamma}(l\kappa, l'\kappa') \frac{p_{l\kappa\alpha}}{m_\kappa} u_{l'\kappa'\gamma}. \quad (10)$$

By using the second quantization form of  $u_{l'\kappa'\gamma}$  and  $p_{l\kappa\alpha}$ , we obtain

$$\begin{aligned} \mathbf{S} &\approx \frac{1}{2V} \frac{i\hbar}{2N} \sum_{l'l'} \sum_{\kappa\kappa'} \sum_{\mathbf{k}\mathbf{k}'} \sum_{\sigma\sigma'} (\mathbf{R}_{l'\kappa'} - \mathbf{R}_{l\kappa}) \\ &\times \sum_{\alpha\gamma} \frac{\Phi_{\alpha\gamma}(l\kappa, l'\kappa')}{\sqrt{m_\kappa m_{\kappa'}}} \epsilon_{\mathbf{k}\sigma\kappa\alpha}^* \epsilon_{\mathbf{k}'\sigma'\kappa'\gamma} \left( \sqrt{\frac{\omega_{\mathbf{k}'\sigma'}}{\omega_{\mathbf{k}\sigma}}} a_{\mathbf{k}\sigma}^\dagger a_{\mathbf{k}\sigma} \right. \\ &\left. + \sqrt{\frac{\omega_{\mathbf{k}\sigma}}{\omega_{\mathbf{k}'\sigma'}}} a_{\mathbf{k}\sigma}^\dagger a_{\mathbf{k}'\sigma'} \right) e^{i(\mathbf{k}' \cdot \mathbf{R}_{l'\kappa'} - \mathbf{k} \cdot \mathbf{R}_{l\kappa})} \times e^{i(\mathbf{k} \cdot \mathbf{d}_\kappa - \mathbf{k}' \cdot \mathbf{d}_{\kappa'})}. \quad (11) \end{aligned}$$

Here  $\mathbf{d}_\kappa$  is the equilibrium position of the  $\kappa$ th atom. We have ignored terms like  $aa$  and  $a^\dagger a^\dagger$ . Using the definition  $\tilde{D}_{\alpha\gamma}(\mathbf{k}', \kappa\kappa') = \sum_{l'} \Phi_{\alpha\gamma}(l\kappa, l'\kappa') e^{i\mathbf{k}' \cdot (\mathbf{R}_{l'\kappa'} - \mathbf{R}_{l\kappa})} / \sqrt{m_\kappa m_{\kappa'}}$ ,

$\tilde{\epsilon}_{\mathbf{k}'\sigma'\kappa'\gamma} = \epsilon_{\mathbf{k}'\sigma'\kappa'\gamma} e^{-i\mathbf{k}'\cdot\mathbf{d}_{\kappa'}}$ , Eq. (11) can be written as

$$\mathbf{S} \approx \frac{\hbar}{4V} \sum_{\mathbf{k}} \sum_{\kappa\kappa'} \sum_{\sigma\sigma'} \sum_{\alpha\gamma} \tilde{\epsilon}_{\mathbf{k}\sigma\kappa\alpha}^* \frac{\partial \tilde{\mathbf{D}}_{\alpha\gamma}(\mathbf{k}, \kappa\kappa')}{\partial \mathbf{k}} \tilde{\epsilon}_{\mathbf{k}\sigma'\kappa'\gamma} \\ \times \left( \sqrt{\frac{\omega_{\mathbf{k}\sigma'}}{\omega_{\mathbf{k}\sigma}}} a_{\mathbf{k}\sigma'} a_{\mathbf{k}\sigma}^\dagger + \sqrt{\frac{\omega_{\mathbf{k}\sigma}}{\omega_{\mathbf{k}\sigma'}}} a_{\mathbf{k}\sigma}^\dagger a_{\mathbf{k}\sigma'} \right). \quad (12)$$

Finally Eq. (12) can be divided into the intraband term ( $\mathbf{S}^D$ ) and the interband term ( $\mathbf{S}^{\text{OD}}$ ) as follows:

$$\mathbf{S}^D = \sum_{\mathbf{k}\sigma} \mathbf{s}_{\mathbf{k}\sigma} \left[ a_{\mathbf{k}\sigma}^\dagger a_{\mathbf{k}\sigma} + \frac{1}{2} \right], \quad (13a)$$

$$\mathbf{S}^{\text{OD}} = \sum_{\mathbf{k}} \sum_{\sigma \neq \sigma'} \mathbf{s}_{\mathbf{k}\sigma\sigma'} a_{\mathbf{k}\sigma}^\dagger a_{\mathbf{k}\sigma'}, \quad (13b)$$

where

$$\mathbf{s}_{\mathbf{k}\sigma} = \frac{\hbar}{2V} \tilde{\epsilon}_{\mathbf{k}\sigma}^\dagger \frac{\partial \tilde{\mathbf{D}}(\mathbf{k})}{\partial \mathbf{k}} \tilde{\epsilon}_{\mathbf{k}\sigma}, \quad (14a)$$

$$\mathbf{s}_{\mathbf{k}\sigma\sigma'} = \frac{\hbar}{4V} \tilde{\epsilon}_{\mathbf{k}\sigma}^\dagger \frac{\partial \tilde{\mathbf{D}}(\mathbf{k})}{\partial \mathbf{k}} \tilde{\epsilon}_{\mathbf{k}\sigma'} \left( \sqrt{\frac{\omega_{\mathbf{k}\sigma'}}{\omega_{\mathbf{k}\sigma}}} + \sqrt{\frac{\omega_{\mathbf{k}\sigma}}{\omega_{\mathbf{k}\sigma'}}} \right). \quad (14b)$$

It has been proved that  $\mathbf{s}_{\mathbf{k}\sigma} = \frac{1}{V} \hbar \omega_{\mathbf{k}\sigma} \mathbf{v}_{\mathbf{k}\sigma}$ , which recovers the conventional heat current operator [30], where  $\mathbf{v}_{\mathbf{k}\sigma}$  is the phonon group velocity.

If the temperature variation  $\delta T(x)$  is weak,  $\beta(x)$  can be written as  $\beta[1 - \delta T(x)/T]$ , where  $(k_B\beta)^{-1}$  is the average temperature  $T$  and  $k_B$  is the Boltzmann constant. Then Eq. (6) becomes  $\rho = e^{-\beta(H+H')}/Z$ , where  $H' = -\frac{1}{T} \int d^3x \delta T(x) h(x)$  formally plays the role of a perturbation. Using the integrated form of Eq. (7), the perturbation due to the temperature gradi-

ent ( $\nabla T$ ) is

$$H' = - \sum_{\nu} \frac{(\nabla T)_{\nu}}{T} \int_{-\infty}^0 dt \int d^3x S_{\nu}(x, t). \quad (15)$$

The density matrix can be expanded in powers of the perturbation by  $e^{-\beta(H+H')} = e^{-\beta H} + e^{-\beta H} \int_0^{\beta} d\lambda e^{\lambda H} H' e^{-\lambda H} + \dots = \rho_0 + \rho_1$  with parameter  $\lambda$ . It is obvious that  $\text{tr} \rho_0 L_{\mu} \equiv 0$ , and the mean PAM is determined by  $\text{tr} \rho_1 L_{\mu}$ , which is

$$\langle L_{\mu} \rangle = -V \sum_{\nu} \frac{(\nabla T)_{\nu}}{T} \sum_n \frac{e^{-\beta E_n}}{Z} \int_0^{\beta} d\lambda \int_{-\infty}^0 dt \\ \times \langle e^{\lambda H} S_{\nu}(t) e^{-\lambda H} L_{\mu}(0) \rangle, \quad (16)$$

where  $e^{\lambda H} S e^{-\lambda H} = S(-i\hbar\lambda)$ , and  $E_n$  is the energy of state  $(\mathbf{k}, \sigma)$  which is noted as  $n$  for short. Then the Kubo formula for PAM can be obtained as [31,32]

$$\langle L_{\mu}(\omega) \rangle = -V \sum_{\nu} \frac{(\nabla T)_{\nu}}{T} \sum_n \frac{e^{-\beta E_n}}{Z} \int_0^{\beta} d\lambda \int_0^{\infty} dt \\ \times e^{i(\omega+i\eta)t} \langle S_{\nu}(-i\hbar\lambda) L_{\mu}(t) \rangle. \quad (17)$$

Here  $\omega$  represents the frequency of an ac temperature gradient. In a perfect crystal,  $\eta$  is an infinitesimal value which goes to zero when  $V \rightarrow \infty$ , corresponding to the infinite lifetime of the phonon. In real materials, we assign  $\eta$  as the relaxation rate, which is the inverse of the relaxation time ( $\tau$ ), when calculating the intraband PAM and assign  $\eta$  as a value larger than the mean level spacing when calculating the interband PAM, respectively [31]. This Kubo expression can be written in the Lehman representation as follows:

$$\langle L_{\mu}(\omega) \rangle = -V \sum_{\nu} \frac{(\nabla T)_{\nu}}{T} \sum_{n,m} \frac{e^{-\beta E_n}}{Z} \int_0^{\beta} d\lambda \int_0^{\infty} dt e^{i(\omega+i\eta)t} \langle n | e^{\lambda H} S_{\nu} e^{-\lambda H} | m \rangle \langle m | e^{\frac{i\hbar t}{\hbar}} L_{\mu} e^{-\frac{i\hbar t}{\hbar}} | n \rangle \\ = V \sum_{\nu} \frac{(\nabla T)_{\nu}}{T} \sum_{n,m} \frac{e^{-\beta E_n}}{Z} \left[ \frac{e^{\beta(E_n - E_m)} - 1}{E_n - E_m} \right] \left( \frac{i\hbar}{E_n - E_m - \hbar\omega - i\hbar\eta} \right) \langle n | S_{\nu} | m \rangle \langle m | L_{\mu} | n \rangle. \quad (18)$$

This expression can be divided into two parts: the contribution from intraband terms  $\langle L_{\mu}^D(\omega) \rangle$  when  $n = m$  and the contribution from interband term  $\langle L_{\mu}^{\text{OD}}(\omega) \rangle$  when  $n \neq m$ :

$$\langle L_{\mu}^{\text{OD}}(\omega) \rangle = V \sum_{\nu} \frac{(\nabla T)_{\nu}}{T} \sum_{nm} \frac{e^{-\beta E_n}}{Z} \left[ \frac{e^{\beta(E_n - E_m)} - 1}{E_n - E_m} \right] \left( \frac{i\hbar}{E_n - E_m - \hbar\omega - i\hbar\eta} \right) \\ \times \sum_{\mathbf{k}\mathbf{k}'\sigma\sigma'\sigma''\sigma'''} \langle n | a_{\mathbf{k}'\sigma''}^\dagger a_{\mathbf{k}\sigma'''} | m \rangle \langle m | a_{\mathbf{k}\sigma}^\dagger a_{\mathbf{k}\sigma'} | n \rangle (\mathbf{s}_{\mathbf{k}'\sigma''\sigma'''} )_{\nu} l_{\mathbf{k}\sigma\sigma'}^{\mu}. \quad (19)$$

The exact state  $|m\rangle$  is the unique state which couples to  $a_{\mathbf{k}\sigma}^\dagger a_{\mathbf{k}\sigma'} |n\rangle$ , denoted as  $|n_{\mathbf{k}\sigma'\sigma}\rangle$ . We can use the standard expressions  $\langle m | a_{\mathbf{k}\sigma}^\dagger a_{\mathbf{k}\sigma'} | n \rangle = \sqrt{(n_{\mathbf{k}\sigma} + 1) n_{\mathbf{k}\sigma'}} \delta_{m n_{\mathbf{k}\sigma'\sigma}}$  and  $\langle n | a_{\mathbf{k}'\sigma''}^\dagger a_{\mathbf{k}\sigma'''} | n_{\mathbf{k}\sigma'\sigma} \rangle = \sqrt{(n_{\mathbf{k}\sigma} + 1) n_{\mathbf{k}\sigma'}} \delta_{\sigma''\sigma} \delta_{\sigma'''\sigma'} \delta_{\mathbf{k}\mathbf{k}'}$ . In terms of the normal mode frequencies,  $E_n - E_m$  becomes  $\hbar(\omega_{\mathbf{k}\sigma'} - \omega_{\mathbf{k}\sigma})$ , where  $\sigma'' = \sigma'$  and  $\sigma''' = \sigma$ . Since  $\sigma \neq \sigma'$ , we can write  $\sum_n \frac{e^{-\beta E_n}}{Z} n_{\mathbf{k}\sigma'} (n_{\mathbf{k}\sigma} + 1) = \langle (n_{\mathbf{k}\sigma} + 1) n_{\mathbf{k}\sigma'} \rangle = \langle n_{\mathbf{k}\sigma'} \rangle \langle (n_{\mathbf{k}\sigma} + 1) \rangle$ . Using the identity  $[e^{\beta\hbar(\omega_{\mathbf{k}\sigma'} - \omega_{\mathbf{k}\sigma})} - 1] \langle n_{\mathbf{k}\sigma'} \rangle \langle (n_{\mathbf{k}\sigma} + 1) \rangle = \langle n_{\mathbf{k}\sigma} \rangle - \langle n_{\mathbf{k}\sigma'} \rangle = n_{\mathbf{k}\sigma}^0 - n_{\mathbf{k}\sigma'}^0$ , with  $n_{\mathbf{k}\sigma}^0$  being the Bose distribution function, the interband term of the mean PAM can be obtained by  $\sigma \leftrightarrow \sigma'$ . The physical meaning of Eq. (19) is that the polarization vector changes when a phonon jumps from one branch to another. Then the rotation of the atom, which is characterized by the phase shift in Eq. (1), is also changed.

Considering  $\langle m | a_{\mathbf{k}\sigma}^\dagger a_{\mathbf{k}\sigma} | n \rangle = n_{\mathbf{k}\sigma} \delta_{mn}$ , the contribution from the intraband term can be written as

$$\langle L_{\mu}^D(\omega) \rangle = -V \beta \sum_{\nu} \frac{(\nabla T)_{\nu}}{T} \left( \frac{i}{\omega + i\eta} \right) \sum_{\mathbf{k}\mathbf{k}'\sigma\sigma''} \left[ \langle n_{\mathbf{k}'\sigma''} n_{\mathbf{k}\sigma} \rangle (\mathbf{s}_{\mathbf{k}'\sigma''})_{\nu} l_{\mathbf{k}\sigma}^{\mu} + \frac{1}{2} \langle n_{\mathbf{k}'\sigma''} \rangle (\mathbf{s}_{\mathbf{k}'\sigma''})_{\nu} l_{\mathbf{k}\sigma}^{\mu} + \frac{1}{2} (\mathbf{s}_{\mathbf{k}'\sigma''})_{\nu} \langle n_{\mathbf{k}\sigma} \rangle l_{\mathbf{k}\sigma}^{\mu} + \frac{1}{4} (\mathbf{s}_{\mathbf{k}'\sigma''})_{\nu} l_{\mathbf{k}\sigma}^{\mu} \right]. \quad (20)$$

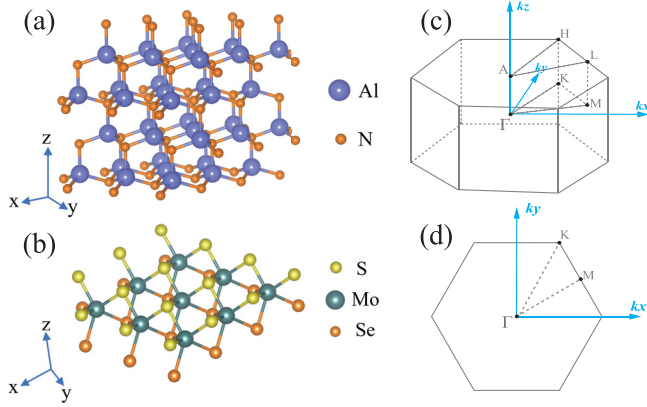


FIG. 1. Crystal structures: (a) wurtzite AlN and (b) MoSSe. (c) and (d) The first Brillouin zones of AlN and MoSSe.

According to Wick's theorem, the factor  $\langle n_{\mathbf{k}'\sigma'} n_{\mathbf{k}\sigma} \rangle$  can be written as  $\langle n_{\mathbf{k}'\sigma'} \rangle \langle n_{\mathbf{k}\sigma} \rangle$  plus a correction  $\langle n_{\mathbf{k}\sigma} \rangle (\langle n_{\mathbf{k}\sigma} \rangle + 1)$ . Using the condition of zero average energy current and zero PAM in equilibrium and the identity  $\langle n_{\mathbf{k}\sigma} \rangle (\langle n_{\mathbf{k}\sigma} \rangle + 1) = -k_B T \frac{\partial \langle n_{\mathbf{k}\sigma} \rangle}{\partial (\hbar\omega_{\mathbf{k}\sigma})}$ , the intraband term of the mean PAM can be obtained by dropping the last three terms in the bracket in Eq. (20). Then, we can obtain the mean PAM per unit volume as  $\langle \mathcal{L}_\mu(\omega) \rangle = \langle \mathcal{L}_\mu^D(\omega) \rangle + \langle \mathcal{L}_\mu^{OD}(\omega) \rangle$ . The intraband part  $\langle \mathcal{L}_\mu^D(\omega) \rangle = \langle L_\mu^D(\omega) \rangle / V$  and the interband part  $\langle \mathcal{L}_\mu^{OD}(\omega) \rangle = \langle L_\mu^{OD}(\omega) \rangle / V$  are written as follows:

$$\begin{aligned} \langle \mathcal{L}_\mu^D(\omega) \rangle &= \sum_v \frac{i(\nabla T)_v}{T} \frac{1}{\omega + i\eta} \sum_{\mathbf{k}\sigma} \frac{\partial n_{\mathbf{k}\sigma}^0}{\partial (\hbar\omega_{\mathbf{k}\sigma})} (\mathbf{s}_{\mathbf{k}\sigma})_v l_{\mathbf{k}\sigma}^\mu \\ &= \sum_v \Lambda_{\mu\nu}^D(\omega) \frac{\partial T}{\partial x_\nu}, \end{aligned} \quad (21a)$$

$$\begin{aligned} \langle \mathcal{L}_\mu^{OD}(\omega) \rangle &= - \sum_v \frac{i(\nabla T)_v}{T} \\ &\times \sum_{\mathbf{k}\sigma\sigma'} \frac{n_{\mathbf{k}\sigma}^0 - n_{\mathbf{k}\sigma'}^0}{\hbar(\omega_{\mathbf{k}\sigma} - \omega_{\mathbf{k}\sigma'})} \frac{(\mathbf{s}_{\mathbf{k}\sigma\sigma'})_v l_{\mathbf{k}\sigma'\sigma}^\mu}{\omega_{\mathbf{k}\sigma} - \omega_{\mathbf{k}\sigma'} - \omega - i\eta} \\ &= \sum_v \Lambda_{\mu\nu}^{OD}(\omega) \frac{\partial T}{\partial x_\nu}, \end{aligned} \quad (21b)$$

where  $\Lambda_{\mu\nu}^D(\omega)$  and  $\Lambda_{\mu\nu}^{OD}(\omega)$  are the intraband response tensor and the interband response tensor, respectively.

#### IV. RESULTS AND DISCUSSIONS

In order to exemplify our theory, we calculate the response tensors of the wurtzite AlN and the monolayer MoSSe, whose lattice structures and first Brillouin zones are depicted in Fig. 1, respectively, in the dc limit ( $\omega \rightarrow 0$ ). The phonon dispersion analysis was performed by using the Vienna *ab initio* simulation package (VASP) [33] with the projector augmented-wave method [34] and the PHONOPY code [35].

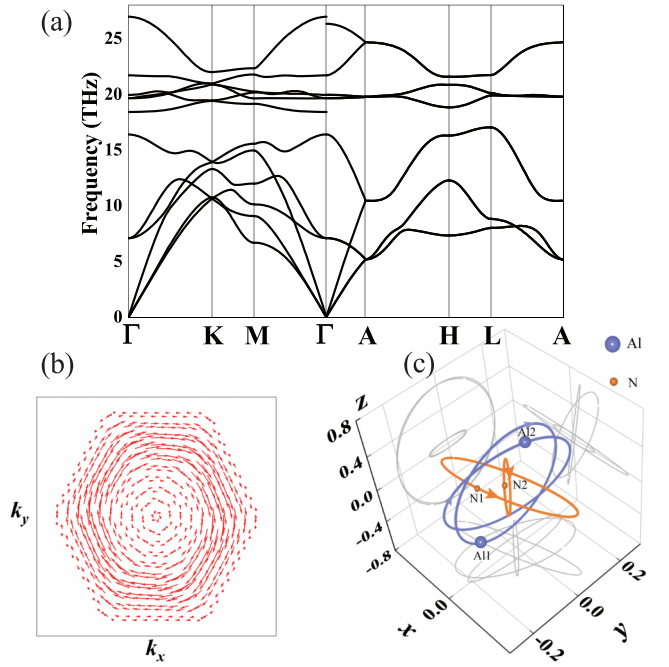


FIG. 2. (a) Phonon dispersion of the wurtzite AlN. (b) Distribution of PAM of the sixth branch on the plane  $k_z = 0$ . (c) Trajectories of the four atoms in the unit cell of the sixth phonon branch at  $\mathbf{k} = (0, 0.5828, 0)(\text{\AA}^{-1})$ . The axes are expressed in dimensionless units.

##### A. Wurtzite AlN

First, we calculate the phonon dispersion of AlN. The nonanalytical term correction in the PHONOPY code is used and the optimized lattice constants are  $a = 3.112 \text{ \AA}$  and  $c = 4.983 \text{ \AA}$ . The generalized gradient approximation with the Perdew-Burke-Ernzerhof [36] realization is adopted for the exchange-correlation function and the plane-wave energy cutoff is set to be 800 eV. For the Born effective charge calculations, the  $k$  points are set to  $17 \times 17 \times 10$  and the corresponding Born effective charges are  $Z_{\text{Al},xx}^* = Z_{\text{Al},yy}^* = 2.517 e$  and  $Z_{\text{Al},zz}^* = 2.677 e$ . For the first-principles harmonic phonon calculations, we used the finite displacement method to get the second-order force constants. In the calculation,  $4 \times 4 \times 2$  supercells (128 atoms) are built and the  $k$ -point mesh is reduced as  $4 \times 4 \times 2$ .

Figure 2(a) shows the calculated phonon dispersion of AlN, which is in agreement with previous works [37]. Figure 2(b) shows the mode-specific PAM ( $\mathbf{l}_{\mathbf{k}\sigma}$ ) of the sixth phonon band when  $k_z = 0$ . We find that the PAM has a chiral texture which mainly consists of tangential components in momentum space. The trajectories of atoms in the sixth phonon branch are shown in Fig. 2(c). It is clear that both aluminum atoms and nitrogen atoms rotate elliptically.

Based on the calculation results in Fig. 2, we are able to calculate the response tensor of AlN as shown in Fig. 3. According to the restriction of the point-group symmetry, the response tensor of the wurtzite AlN (point group:  $C_{6v}$ ) has only one independent nonzero element  $\Lambda_{xy}$ . It can be divided into two parts: the intraband contribution  $\Lambda_{xy}^D$  and the interband contributions  $\Lambda_{xy}^{OD}$ . The calculation results show that the

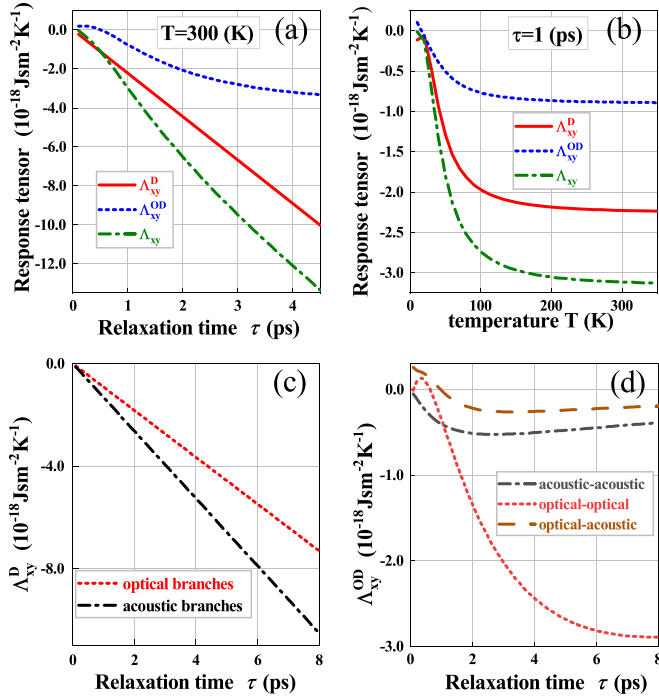


FIG. 3. PAM response tensor  $\Lambda_{xy}$  of the wurtzite AlN. (a) The intraband part  $\Lambda_{xy}^D$  (red solid line), the interband part  $\Lambda_{xy}^{OD}$  (blue dashed line), and the total contribution  $\Lambda_{xy}$  (green dotted line) as functions of the relaxation time  $\tau$  when  $T = 300 \text{ K}$ . (b)  $\Lambda_{xy}^D$  (red solid line),  $\Lambda_{xy}^{OD}$  (blue dashed line), and  $\Lambda_{xy}$  (green dotted line) versus the temperature  $T$  when  $\tau = 1 \text{ ps}$ . (c) The contribution of acoustic branches (black dotted line) and optical branches (red dotted line) to the intraband part  $\Lambda_{xy}^D$ . (d) The contribution to the interband part  $\Lambda_{xy}^{OD}$  from the transitions between different phonon branches.

amplitude of the PAM response tensor  $|\Lambda_{xy}|$  increases with the increase of the relaxation time  $\tau$  as shown in Fig. 3(a). As for the intraband part,  $\Lambda_{xy}^D$  varies linearly with  $\tau$ , which is the same as the Boltzmann transport equation calculations [14]. As for the interband part, we find that it also has a nonzero contribution, albeit a weak one in the case of the wurtzite AlN. Figure 3(b) shows the temperature dependence of response tensors at  $\tau = 1 \text{ ps}$ . One can see that both  $|\Lambda_{xy}^D|$  and  $|\Lambda_{xy}^{OD}|$  decrease dramatically when the temperature decreases. A sign change of  $\Lambda_{xy}^{OD}$  is found around 20 K. With the increase of temperature, both  $\Lambda_{xy}^D$  and  $\Lambda_{xy}^{OD}$  show a moderate overall downward trend and eventually approach the high-temperature limit when  $T$  becomes comparable to the Debye temperature.

We now distinguish the contributions from different phonon branches to  $\Lambda_{xy}^D$  in Fig. 3(c) and the contributions from different interband phonon transitions to  $\Lambda_{xy}^{OD}$  in Fig. 3(d), respectively. For  $\Lambda_{xy}^D$ , we find that the contribution from the acoustic branch is more significant than the contribution from the optical branch. The reason is that the acoustic branch has a greater phonon group velocity which is included in  $s_{\mathbf{k}\sigma}$  in Eq. (21a). For  $\Lambda_{xy}^{OD}$ , we plot the calculated acoustic-acoustic transition, acoustic-optical transition, and optical-optical transition components of  $\Lambda_{xy}^{OD}$ . The calculation results show that the quantum transition between the two optical branches is

dominant. The contribution from quantum transitions between the two acoustic branches and that between one acoustic branch and one optical branch are relatively small. This is because of the closeness of phonon energies between optical bands, which is preferred for interband transition, as shown in Fig. 2(a).

In order to intuitively present the nonzero PAM of the wurtzite AlN, we compare the numerically calculated PAM with a rotating rigid body. By setting  $\tau \sim 4 \text{ ps}$  at room temperature [38], one can obtain that  $\Lambda_{xy}^D = -8.91 \times 10^{-18} \text{ Jsm}^{-2} \text{ K}^{-1}$  and  $\Lambda_{xy}^{OD} = -3.21 \times 10^{-18} \text{ Jsm}^{-2} \text{ K}^{-1}$ . Let us consider a cubic sample with the length of side  $\ell$  whose moment of inertia  $I = \frac{1}{6}M\ell^2$ , where  $M$  is the mass of the sample. When a temperature gradient along the  $y$  direction  $(\nabla T)_y$  is applied, the angular velocity in the  $x$  direction  $(\omega_x)$  of the rigid body rotation, which is equivalent to the generated PAM, is  $\omega_x = \frac{-\Lambda_{xy}(\nabla T)_y}{\frac{1}{6}\rho\ell^2}$ , where  $\rho$  is the mass density. If  $(\nabla T)_y = 10^6 \text{ K/m}$ ,  $\ell = 10 \mu\text{m}$ , and  $\rho = 3.2 \text{ g/cm}^3$ , we find  $\omega_x = 2.27 \times 10^{-4} \text{ s}^{-1}$ .

## B. The monolayer MoS<sub>2</sub>

We now turn to investigate the monolayer MoS<sub>2</sub>, a Janus transition metal dichalcogenides, where the top-layer S atoms of MoS<sub>2</sub> are replaced by Se atoms [39]. The optimized lattice constant is  $a = 3.251 \text{ \AA}$  [40]. The vacuum slab in the  $z$  direction is set to  $c = 18.419 \text{ \AA}$  in order to avoid the interaction between neighboring layers. The bond lengths of Mo-Se and Mo-S are 2.535 and 2.420  $\text{\AA}$ , respectively. The energy cutoff is fixed to 600 eV. The force constants are calculated by the VASP-DFPT method, and the Brillouin zone is sampled with a  $4 \times 4 \times 1$   $\Gamma$ -point centered grid.

Calculated phonon dispersion of MoS<sub>2</sub> is in agreement with previous work [41] as shown in Fig. 4(a). Figure 4(b) plots the PAM of the sixth phonon branch. The PAM texture of MoS<sub>2</sub> exhibits chirality near the center of the Brillouin zone and has  $z$  components near the Brillouin zone boundary. We then calculate the trajectories of three atoms in the unit cell for the sixth branch at high-symmetry point K as shown in Fig. 4(c). This point is chosen because the normalized trajectory at this point has a threefold rotational symmetry exhibiting the intrinsic circular polarization characteristics of chiral phonons.

Figure 5 shows the calculated response tensor of MoS<sub>2</sub>. Its point group  $C_{3v}$  leads to a PAM response tensor with only a single independent element  $\Lambda_{xy}$ .  $\Lambda_{xy}$  at  $T = 300 \text{ K}$  with  $\tau$  ranging from 0.1 to 10 ps is shown in Fig. 5(a). One can see that  $\Lambda_{xy}^{OD}$  is negative and  $\Lambda_{xy}^D$  is positive. The overall response tensor is dominated by  $\Lambda_{xy}^{OD}$  when  $\tau < 8 \text{ ps}$ . We also find that  $|\Lambda_{yx}^{OD}|$  increases first and then decreases with increasing  $\tau$ , while  $\Lambda_{xy}^D$  always increases. The extreme value of  $|\Lambda_{yx}^{OD}|$  is determined by  $\tau^{-1} \sim \omega_{\mathbf{k}\sigma} - \omega_{\mathbf{k}\sigma'}$ . Figure 5(b) shows the temperature dependence of response tensors when  $\tau = 1 \text{ ps}$ . As the temperature increases,  $\Lambda_{xy}^D$  rises rapidly and then decreases gradually until it reaches the high-temperature limit  $-1.27 \times 10^{-18} \text{ Jsm}^{-2} \text{ K}^{-1}$ .  $\Lambda_{xy}^{OD}$  exhibits a sharp decrease and eventually reaches  $-3.43 \times 10^{-17} \text{ Jsm}^{-2} \text{ K}^{-1}$ .

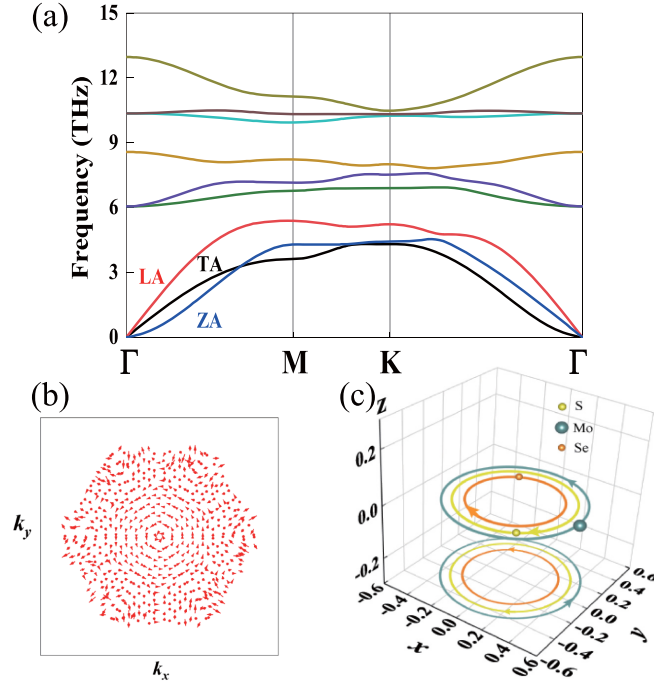


FIG. 4. (a) Phonon dispersion of the monolayer MoSSe. (b) Distribution of the PAM of the sixth branch. (c) Trajectories of tree atoms in the unit cell of the sixth phonon branch at high-symmetry point K, which represents the normalized polarization vector, and the axes are expressed in dimensionless units.

In Figs. 5(c) and 5(d), we distinguish the contributions to  $\Lambda_{xy}^D$  from different phonon branches and the contribution to  $\Lambda_{xy}^{OD}$  from different interband transitions. The contribution from acoustic phonon branches to  $\Lambda_{xy}^D$  is slightly larger than that from optical phonon branches. As for  $\Lambda_{xy}^{OD}$ , the transition between two acoustic branches is dominant. The contribution from transitions between two optical branches and that between one acoustic branch and one optical branch are relatively small.

Finally, we compare the PAM generated by a temperature gradient with a rotating rigid body. Assuming that the phonon relaxation time is 10 ps. The corresponding  $\Lambda_{xy}^D$  and  $\Lambda_{xy}^{OD}$  are  $1.27 \times 10^{-17} \text{ Jsm}^{-2} \text{ K}^{-1}$  and  $-8.56 \times 10^{-18} \text{ Jsm}^{-2} \text{ K}^{-1}$  in our results. Let us consider a disk with radius  $\mathfrak{R}$  whose moment of inertia  $I = \frac{1}{2}M\mathfrak{R}^2$ . The angular velocity is expressed as  $\omega_x = \frac{-\Lambda_{xy}(\nabla T)_y}{\frac{1}{2}\rho\mathfrak{R}^2}$ . If  $(\nabla T)_y = 10^6 \text{ K/m}$ ,  $\mathfrak{R} = 10 \text{ }\mu\text{m}$ , and  $\rho = 5.24 \text{ g/cm}^3$ , the angular velocity  $\omega_x$  of the rigid body rotation is estimated as  $\omega_x = -1.58 \times 10^{-5} \text{ s}^{-1}$ .

## V. SUMMARY AND OUTLOOK

In summary, the Kubo formula is used to calculate the PAM induced by a temperature gradient, and the response tensors for the wurtzite AlN and the monolayer MoSSe are calculated as examples. It is found that interband phonon transitions play a significant role in generating nonzero PAM. In addition, we point out that interband PAM could be further enhanced in nonperfect crystals where momentum conservation is absent. In other words, the transition between  $(\mathbf{k}, \sigma)$

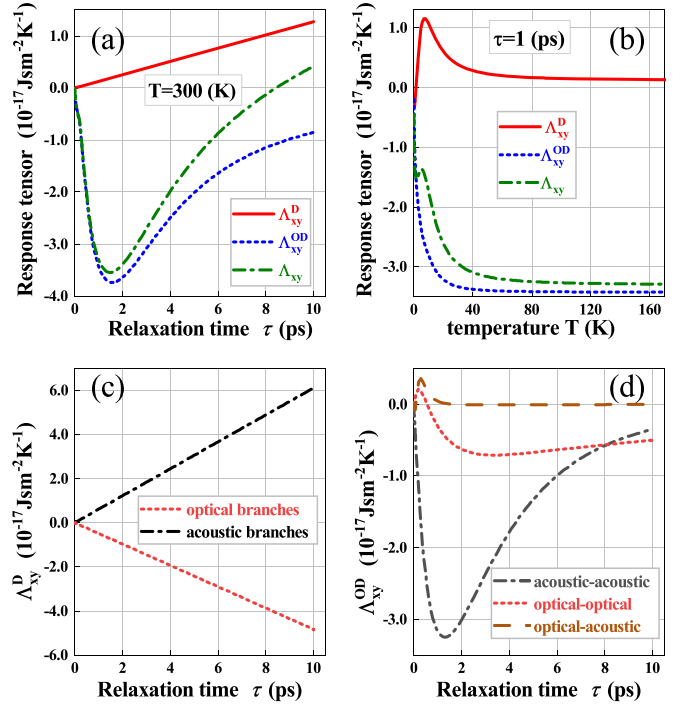


FIG. 5. Calculated PAM response tensor  $\Lambda_{xy}$  of the monolayer MoSSe. (a) The intraband part  $\Lambda_{xy}^D$  (red solid line), the interband part  $\Lambda_{xy}^{OD}$  (blue dashed line), and  $\Lambda_{xy}$  (green dotted line) as functions of the relaxation time  $\tau$  when  $T = 300 \text{ K}$ . (b)  $\Lambda_{xy}^D$  (red solid line),  $\Lambda_{xy}^{OD}$  (blue dashed line), and  $\Lambda_{xy}$  (green dotted line) versus  $T$  when  $\tau = 1 \text{ ps}$ . (c) The contribution from acoustic branches (black dotted line) and optical branches (red dotted line) to  $\Lambda_{xy}^D$ . (d) The contribution to the interband part  $\Lambda_{xy}^{OD}$  from the transitions between different phonon branches.

and  $(\mathbf{k}', \sigma')$  should be also considered. Moreover, the anharmonic properties are described using a simple constant relaxation time approximation, but for systems with strong phonon scattering, the dependence of a phonon's lifetime on the wave vector  $\mathbf{k}$  and the phonon linewidth should be considered. Interband transitions of phonons are critical for thermal transport in amorphous [32] or complex crystals [42–44] with strong anharmonicity, as discussed in previous works [45,46] on lattice thermal conductivity. Therefore, our work provides a possible preliminary interpretation of the experiment [23] since the extremely low thermal conductivity of the chiral organic-inorganic hybrid perovskites used in the experiment implies that the interband contribution could be important. It is worth noting that chiral organic-inorganic hybrid perovskites are a possible candidate for observing a large PAM and phonon magnetic moment.

## ACKNOWLEDGMENTS

This work was supported by the National Natural Science Foundation of China (Grants No. 11890703 and No. 12275133). J.Z. is also supported by the ‘‘Shuangchuang’’ Doctor program of Jiangsu Province (Grant No. JSS-CBS20210341).

- [1] N. W. Ashcroft and N. D. Mermin, *Solid State Physics* (Harcourt, Inc., Orlando, 1976), p. 453.
- [2] M. Born and K. Huang, *Dynamical Theory of Crystal Lattices* (Oxford University, London, 1954).
- [3] J. Callaway, *Quantum Theory of the Solid State* (Academic Press, San Diego, 1991).
- [4] G. Schaack, *J. Phys. C: Solid State Phys.* **9**, L297 (1976).
- [5] E. Anastassakis, E. Burstein, A. Maradudin, and R. Minnick, *J. Phys. Chem. Solids* **33**, 519 (1972).
- [6] H. Zhu, J. Yi, M. Li, J. Xiao, L. Zhang, C. Yang, R. A. Kaindl, L. Li, Y. Wang, and X. Zhang, *Science* **359**, 579 (2018).
- [7] L. Zhang and Q. Niu, *Phys. Rev. Lett.* **112**, 085503 (2014).
- [8] L. Zhang and Q. Niu, *Phys. Rev. Lett.* **115**, 115502 (2015).
- [9] A. G. McLellan, *J. Phys. C: Solid State Phys.* **21**, 1177 (1988).
- [10] A. Holz, *Nuovo Cimento B* **9**, 83 (1972).
- [11] H. Capellmann and S. Lipinski, *Z. Phys. B: Condens. Matter* **83**, 199 (1991).
- [12] T. Kariyado and Y. Hatsugai, *Sci. Rep.* **5**, 18107 (2015).
- [13] Y.-T. Wang, P.-G. Luan, and S. Zhang, *New J. Phys.* **17**, 073031 (2015).
- [14] M. Hamada, E. Minamitani, M. Hirayama, and S. Murakami, *Phys. Rev. Lett.* **121**, 175301 (2018).
- [15] S. Park and B.-J. Yang, *Nano Lett.* **20**, 7694 (2020).
- [16] Z. Huang, B. P. Bloom, X. Ni, Z. N. Georgieva, M. Marciesky, E. Vetter, F. Liu, D. H. Waldeck, and D. Sun, *ACS Nano* **14**, 10370 (2020).
- [17] Y. Ren, C. Xiao, D. Saporov, and Q. Niu, *Phys. Rev. Lett.* **127**, 186403 (2021).
- [18] B. Cheng, T. Schumann, Y. Wang, X. Zhang, D. Barbalas, S. Stemmer, and N. P. Armitage, *Nano Lett.* **20**, 5991 (2020).
- [19] T. F. Nova, A. Cartella, A. Cantaluppi, M. Först, D. Bossini, R. V. Mikhaylovskiy, A. Kimel, R. Merlin, and A. Cavalleri, *Nat. Phys.* **13**, 132 (2017).
- [20] D. M. Juraschek, M. Fechner, A. V. Balatsky, and N. A. Spaldin, *Phys. Rev. Mater.* **1**, 014401 (2017).
- [21] D. M. Juraschek and N. A. Spaldin, *Phys. Rev. Mater.* **3**, 064405 (2019).
- [22] S. R. Tauchert, M. Volkov, D. Ehberger, D. Kazenwadel, M. Evers, H. Lange, A. Donges, A. Book, W. Kreuzpaintner, U. Nowak *et al.*, *Nature (London)* **602**, 73 (2022).
- [23] K. Kim, E. Vetter, L. Yan, C. Yang, Z. Wang, R. Sun, Y. Yang, A. H. Comstock, X. Li, J. Zhou *et al.*, *Nat. Mater.* **22**, 322 (2023).
- [24] G. Xiong, H. Chen, D. Ma, and L. Zhang, *Phys. Rev. B* **106**, 144302 (2022).
- [25] M. Hamada, Ph.D. thesis, Tokyo Institute of Technology, 2021.
- [26] R. Kubo, M. Yokota, and S. Nakajima, *J. Phys. Soc. Jpn.* **12**, 1203 (1957).
- [27] R. Zwanzig, *Annu. Rev. Phys. Chem.* **16**, 67 (1965).
- [28] H. Mori, I. Oppenheim, and J. Ross, *Studies in Statistical Mechanics*, Vol. 1 (North Holland, Amsterdam, 1962), p. 213.
- [29] R. Kubo, *J. Phys. Soc. Jpn.* **12**, 570 (1957).
- [30] R. J. Hardy, *Phys. Rev.* **132**, 168 (1963).
- [31] P. B. Allen and J. L. Feldman, *Phys. Rev. Lett.* **62**, 645 (1989).
- [32] P. B. Allen and J. L. Feldman, *Phys. Rev. B* **48**, 12581 (1993).
- [33] G. Kresse and J. Furthmüller, *Phys. Rev. B* **54**, 11169 (1996).
- [34] G. Kresse and D. Joubert, *Phys. Rev. B* **59**, 1758 (1999).
- [35] A. Togo and I. Tanaka, *Scr. Mater.* **108**, 1 (2015).
- [36] J. P. Perdew, K. Burke, and M. Ernzerhof, *Phys. Rev. Lett.* **77**, 3865 (1996).
- [37] C. Bungaro, K. Rapcewicz, and J. Bernholc, *Phys. Rev. B* **61**, 6720 (2000).
- [38] A. AlShaikhi and G. P. Srivastava, *Phys. Rev. B* **76**, 195205 (2007).
- [39] A.-Y. Lu, H. Zhu, J. Xiao, C.-P. Chuu, Y. Han, M.-H. Chiu, C.-C. Cheng, C.-W. Yang, K.-H. Wei, Y. Yang *et al.*, *Nat. Nanotechnol.* **12**, 744 (2017).
- [40] S.-D. Guo, *Phys. Chem. Chem. Phys.* **20**, 7236 (2018).
- [41] M. M. Petrić, M. Kremser, M. Barbone, Y. Qin, Y. Sayyad, Y. Shen, S. Tongay, J. J. Finley, A. R. Botello-Méndez, and K. Müller, *Phys. Rev. B* **103**, 035414 (2021).
- [42] Y. Wang, R. Lin, P. Zhu, Q. Zheng, Q. Wang, D. Li, and J. Zhu, *Nano Lett.* **18**, 2772 (2018).
- [43] A. Pisoni, J. Jaćimović, O. S. Barišić, M. Spina, R. Gaál, L. Forró, and E. Horváth, *J. Phys. Chem. Lett.* **5**, 2488 (2014).
- [44] W. Lee, H. Li, A. B. Wong, D. Zhang, M. Lai, Y. Yu, Q. Kong, E. Lin, J. J. Urban, J. C. Grossman *et al.*, *Proc. Natl. Acad. Sci. USA* **114**, 8693 (2017).
- [45] Y. Xia, *Appl. Phys. Lett.* **113**, 073901 (2018).
- [46] G. Caldarelli, M. Simoncelli, N. Marzari, F. Mauri, and L. Benfatto, *Phys. Rev. B* **106**, 024312 (2022).